Molecular and Crystal Structure of 3,3-Bis(triethylphosphine)-1,2-dicarba-3-platinadodecaborane(11), and Molecular-orbital Analysis of the ' Slip ' Distortion in Carbametallaboranes †

By **D. Michael P. Mingos** * and **Michael I. Forsyth**, Inorganic Chemistry Laboratory, South Parks Road, Oxford OX1 3QR
Alan J. Welch, Department of Inorganic Chemistry, The University, Bristol BS8 1TS

Crystals of the title compound are monoclinic, space group $P2_1/n$ with unit-cell dimensions a = 9.375(4), b = 15.985(3), c = 16.033(7) Å, and β = 93.56(5)°. The structure has been solved using 6 068 observed reflections recorded at *ca.* 215 K on a four-circle diffractometer, and refined by least squares to R 0.047. The geometry of the cage is that of a highly distorted icosahedron in which the platinum atom ' slips ' towards B(8) and the metal-bonded face ' folds ' across B(4) · · · B(7). Molecular-orbital calculations based on the extended-Hückel approximation have accounted for the ' slip ' and ' fold ' distortions observed in this and related carbametallaboranes.

THE ' slip ' distortion in electron-rich carbametallaboranes was first recognised almost a decade ago as a result of an extensive investigation of sandwich complexes derived from the carbaborane ligand 1,2-R_2-1,2-$C_2B_9H_9$.[1-11] These early structural studies defined the ' slip ' distortion in terms of a displacement of the metal atom, from its more usual position above the centroid of the open pentagonal face of the ligand towards the unique boron atom.[9-11] Recently this view of the distortion has been questioned by Wallbridge and his co-workers,[12] who have noted the distinct non-planarity of the C_2B_3 face which is bonded to the metal.

† This paper is regarded as Part 8 in the series ' Metallaborane Chemistry ' (Part 7 of which is ref. 27*b*), and Part 2 in the series ' Molecular-orbital Studies on Carbametallaboranes ' (Part 1 of which is ref. 17).

[1] A. Zalkin, D. H. Templeton, and T. E. Hopkins, *J. Amer. Chem. Soc.*, 1965, **87**, 3988.
[2] A. Zalkin, T. E. Hopkins, and D. H. Templeton, *Inorg. Chem.*, 1966, **5**, 1189.
[3] A. Zalkin, T. E. Hopkins, and D. H. Templeton, *Inorg. Chem.*, 1967, **6**, 1911.
[4] B. G. DeBoer, A. Zalkin, and D. H. Templeton, *Inorg. Chem.*, 1968, **7**, 2288.
[5] M. R. Churchill, K. Gold, J. N. Francis, and M. F. Hawthorne, *J. Amer. Chem. Soc.*, 1969, **91**, 1222.
[6] D. St. Clair, A. Zalkin, and D. H. Templeton, *J. Amer. Chem. Soc.*, 1970, **92**, 1173.
[7] M. R. Churchill and K. Gold, *J. Amer. Chem. Soc.*, 1970, **92**, 1180.
[8] D. St. Clair, A. Zalkin, and D. H. Templeton, *Inorg. Chem.*, 1971, **10**, 2587.
[9] F. V. Hansen, R. G. Hazell, C. Hyatt, and G. D. Stuky, *Acta Chem. Scand.*, 1973, **27**, 1210.
[10] R. M. Wing, *J. Amer. Chem. Soc.*, 1967, **89**, 5599.
[11] R. M. Wing, *J. Amer. Chem. Soc.*, 1968, **90**, 4828.
[12] H. M. Colquhoun, T. J. Greenhough, and M. G. H. Wallbridge, *J.C.S. Chem. Comm.*, 1976, 1019; *Acta Cryst.*, 1977, **B33**, 3604.

The *X*-ray crystallographic studies of these 'dicarbollide' complexes have shown that in general the distortions only become significant when the metal ion has a d^8 or d^9 configuration. The total number of valence electrons is, however, not the only factor governing the magnitude and sense of distortion in these complexes. Wing [13] has noted that the substituents on the open face of the 'dicarbollide' ligand may influence the extent of the 'slip' distortion.

There has been no shortage of explanations to account for the electronic origins of the 'slip' distortion, the following being the most important: (*i*) η-allylic bonding,[11] (*ii*) asymmetric metal–ligand bonding effects,[14] (*iii*) the generation of *nido*-like structures,[15] (*iv*) molecular-orbital (m.o.) schemes based on $[Fe(\eta\text{-}C_5H_5)_2]$,[16] and (*v*) back donation from the metal to the ligand e_2 set.[12]

The recent success achieved in rationalising the conformations of carbaplatinaboranes [17] using extended-Hückel m.o. calculations prompted us to examine in some detail the electronic factors responsible for the 'slip' and related distortions in these molecules. We were also interested in establishing the effect of substituents on the distortion and therefore undertook a crystallographic analysis of 3,3-$(Et_3P)_2$-3,1,2-$PtC_2B_9H_{11}$. This complemented earlier work [18,19] on the compounds 1-Me_3N-2,2-$(Bu^tNC)_2$-2,1-$PdCB_{10}H_{10}$ and 1,1-$(PhMe_2P)_2$-2,4-Me_2-1,2,4-$PtC_2B_9H_9$ which are isoelectronic but have different substitution patterns. The compound 3,3-$(Et_3P)_2$-3,1,2-$PtC_2B_9H_{11}$ forms good-quality crystals and has the advantage that the cage carbon atoms are not methylated, thus reducing the possibility of competing electronic and steric effects. To enhance the distinguishability of the cage atoms the diffraction data were collected at low temperature. Preliminary details of this work have been published,[20] and whilst the work was in progress a crystallographic study of the related compound 3-Et_2NCS_2-3,1,2-$AuC_2B_9H_{11}$ was reported.[12]

EXPERIMENTAL

The compound was recrystallised from methylene chloride–cyclohexane at 5 °C as bright orange transparent blocks, stable in air for indefinite periods. A single crystal, *ca.* 0.03 × 0.025 × 0.025 cm, mounted with an epoxy-resin adhesive on a quartz fibre, was used to establish the unit cell and space group *via* oscillation and equi-inclination Weissenberg photographs taken about *a* (nickel-filtered Cu-K_α radiation).

The specimen was then transferred to a Syntex $P2_1$ four-circle autodiffractometer equipped with ϕ-axis low-temperature device (N_2 stream) and slowly cooled to *ca.* 215 K. When a steady state had been achieved accurate unit-cell dimensions and one quadrisphere of diffracted intensities were recorded following an established procedure.[21] Details pertinent to the present experiment were as follows. In the centring routine, 15 reflections, $16 < 2\theta < 25°$ (Mo-K_α), were taken from a 30′ rotation photograph. The unit cell was chosen to correspond to that determined photographically and the orientation matrix calculated. For data collection, $2.9 \leqslant 2\theta \leqslant 60.0°$ in five shells, using graphite-monochromated Mo-K_α radiation, $\lambda_{\alpha1} = 0.709\ 26$, and $\lambda_{\alpha2} = 0.713\ 54$ Å. Peaks were scanned (θ—2θ in 96 steps) from 1.0° below $K_{\alpha1}$ to 1.0° above $K_{\alpha2}$ at rates between 0.042 5 and 0.488 3° s^{-1}, the precise rate being dependent on an initial 2-s peak count in which 150 and 1 500 counts were used as minimum and maximum thresholds. All the net intensities were thereafter scaled to a common 0.016 7° s^{-1} basis. Three check reflections ($1\bar{7}4$, $\bar{3}53$, and $\bar{1}5\bar{5}$) were remonitored once every 50, but subsequent analysis [22] of their net counts as individual functions of time implied no significant machine variance or crystal decomposition or movement over the *ca.* 204-h *X*-ray exposure. Of 7 044 independent reflections measured ($+h$, $+k$, $\pm l$ with equivalent $0kl$ and $0k\bar{l}$ intensities afterwards merged) 6 289 were retained ($I \geqslant 1.0\sigma$) for structure solution and refinement. External crystal faces were identified as {011, 01$\bar{1}$, 111, 11$\bar{1}$, 1$\bar{1}$1, and $\bar{1}$11} and their inversion-related equivalents and an absorption correction was applied resulting in a range of correction factors of 3.01 (0 0 14) to 3.60 (1 0 1).

Crystal Data.—$C_{14}H_{41}B_9P_2Pt$, $M = 563.8$, Monoclinic, $a = 9.375(4)$, $b = 15.985(3)$, $c = 16.033(7)$ Å, $\beta = 93.56(5)°$, $U = 2\ 398(2)$ Å^3 at *ca.* 215 K, $D_m = 1.56$ (flotation), $Z = 4$, $D_c = 1.561$ g cm^{-3}, $F(000) = 1\ 112$ electrons, μ(Mo-K_α) = 62.85 cm^{-1}, space group $P2_1/n$ (alternative setting of $P2_1/c$, C_{2h}^5, no. 14).

Intensity data were corrected for Lorentz and polarisation effects, and the structure solved *via* Patterson (Pt and P) and iterative full-matrix least-squares refinement and electron-density difference syntheses (C, B, and H). Initially, all the light cage atoms were treated as boron. The true identities of the cage carbons soon became apparent from their post-refinement isotropic thermal parameters and internuclear distances. All the hydrogen atoms were located from a ΔF map computed with those 2 366 data for which $(\sin\theta)/\lambda \leqslant 0.5$, and were positionally but not thermally refined [U_H 0.04 Å^2 (cage H, methylene H), U_H 0.05 Å^2 (methyl H)].

F_o moduli were weighted such that $w^{-1} = xy$ with $x = F_o/a$ if $F_o > a$, $x = 1$ if $F_o \leqslant a$, $y = b/\sin\theta$ if $\sin\theta < b$, and $y = 1$ if $\sin\theta \geqslant b$ in which a and b took the values 80.0 and 0.33 respectively. All the non-hydrogen atoms were allowed anisotropic thermal parameters and the 363 variables (including five F-scale factors) were divided between four blocks. In the final stages of refinement, reflections were included in structure-factor calculations if $I > 2.5\sigma$ (5 700 data) or $1.0 \leqslant I \leqslant 2.5\sigma$ and $|F_c| \geqslant F_o$ (368 data). With the data-to-variable ratio thus better than 16.7 : 1 refinement converged at R 0.047 and R' 0.057. Apart from some residue around the metal atom the final difference Fourier (0.33 Å resolution) appeared featureless.

Atomic scattering factors for neutral atoms were those of

[13] R. M. Wing, *J. Amer. Chem. Soc.*, 1970, **92**, 1187.
[14] L. F. Warren, jun., and M. F. Hawthorne, *J. Amer. Chem. Soc.*, 1968, **90**, 4823.
[15] K. Wade, *Chem. Comm.*, 1971, 792.
[16] P. A. Wegner, *Inorg. Chem.*, 1975, **14**, 212.
[17] D. M. P. Mingos, *J.C.S. Dalton*, 1977, 602.
[18] W. E. Carroll, M. Green, F. G. A. Stone, and A. J. Welch, *J.C.S. Dalton*, 1975, 2263.
[19] A. J. Welch, *J.C.S. Dalton*, 1975, 1473.
[20] D. M. P. Mingos, M. I. Forsyth, and A. J. Welch, *J.C.S. Chem. Comm.*, 1977, 605.
[21] A. G. Modinos and P. Woodward, *J.C.S. Dalton*, 1974, 2065.
[22] A. G. Modinos, DRSYN, a Fortran program for data analysis.

refs. 23 (Pt and B), 24 (P and C), and 25 (H), with appropriate correction [26] for both components of anomalous dispersion. Final atomic co-ordinates are listed in Table 1. Anisotropic temperature factors and a comparison of $10|F_o|$ against $10F_c$ are contained (Appendices A and B) in Supplementary Publication No. SUP 22264 (32 pp.).* All the crystallographic calculations were performed *via* the '*X*-RAY '72' system, implemented on the University of London CDC 7600 computer.

TABLE 1

Final positional parameters (fractional co-ordinates; $\times 10^5$ Pt and P; $\times 10^4$ B and C; $\times 10^3$ H) *

Atom	*x*	*y*	*z*
C(1)	1 482(8)	721(4)	924(4)
C(2)	2 987(7)	849(4)	1 328(4)
Pt(3)	10 886(2)	14 781(1)	22 759(1)
B(4)	427(8)	1 629(5)	890(5)
B(5)	1 241(9)	1 187(5)	−1(5)
B(6)	2 923(9)	698(5)	274(5)
B(7)	3 128(8)	1 877(6)	1 684(5)
B(8)	1 560(9)	2 458(5)	1 311(5)
B(9)	1 415(9)	2 287(5)	208(5)
B(10)	2 900(9)	1 726(5)	−129(5)
B(11)	4 004(8)	1 468(6)	784(5)
B(12)	3 103(9)	2 455(5)	709(5)
P(1)	21 814(18)	16 956(11)	35 646(10)
C(11)	2 872(8)	2 767(5)	3 655(5)
C(111)	1 691(11)	3 428(5)	3 624(7)
C(12)	1 214(9)	1 604(5)	4 527(5)
C(121)	2 111(10)	1 794(7)	5 341(5)
C(13)	3 775(8)	1 050(5)	3 763(5)
C(131)	3 496(12)	117(7)	3 847(8)
P(2)	−9 154(17)	8 165(11)	26 795(11)
C(21)	−597(8)	−150(5)	3 281(5)
C(211)	124(11)	−814(5)	2 766(6)
C(22)	−2 127(7)	1 436(5)	3 282(5)
C(221)	−2 704(10)	2 193(6)	2 802(6)
C(23)	−2 105(7)	443(5)	1 799(4)
C(231)	−3 395(9)	−76(6)	2 030(5)
H(1)	93(13)	12(8)	98(8)
H(2)	348(13)	45(8)	162(8)
H(4)	−65(14)	160(8)	74(8)
H(5)	52(13)	103(8)	−51(8)
H(6)	326(13)	12(8)	5(8)
H(7)	390(13)	206(8)	217(8)
H(8)	113(13)	301(8)	148(8)
H(9)	85(13)	279(8)	−20(8)
H(10)	330(13)	191(8)	−81(8)
H(11)	511(14)	137(8)	88(8)
H(12)	373(13)	306(8)	68(8)
H(111)	355(13)	273(8)	415(8)
H(112)	399(13)	280(8)	321(8)
H(121)	47(13)	196(8)	447(8)
H(122)	87(13)	109(8)	452(8)
H(131)	450(14)	136(8)	340(8)
H(132)	425(14)	129(8)	427(8)
H(211)	9(13)	−6(8)	376(8)
H(212)	−153(13)	−32(8)	349(8)
H(221)	−291(13)	98(8)	343(8)
H(222)	−161(14)	174(8)	375(8)
H(231)	−236(13)	91(8)	151(8)
H(232)	−145(13)	12(8)	143(8)
H(111A)	225(15)	402(9)	380(9)
H(111B)	111(15)	348(9)	416(9)
H(111C)	120(15)	343(9)	319(9)
H(121A)	162(15)	175(9)	582(9)
H(121B)	235(15)	240(9)	532(9)
H(121C)	291(15)	142(9)	546(9)
H(131A)	441(15)	−15(9)	399(9)
H(131B)	299(15)	4(9)	331(9)
H(131C)	313(15)	9(9)	432(9)
H(211A)	−56(15)	−100(9)	234(9)
H(211B)	127(15)	−63(9)	259(9)
H(211C)	28(15)	−121(9)	302(9)
H(221A)	−322(15)	254(9)	310(9)
H(221B)	−325(15)	209(9)	231(9)
H(221C)	−197(15)	261(9)	275(9)
H(231A)	−400(15)	−21(9)	149(9)
H(231B)	−405(14)	22(9)	233(8)
H(231C)	−319(15)	−67(9)	238(8)

* Estimated standard deviations are expressed in parentheses throughout this paper.

DISCUSSION

The compound 3,3-$(Et_3P)_2$-3,1,2-$PtC_2B_9H_{11}$ crystallises as discrete, neutral, monomeric molecules with no imposed symmetry. A perspective view of a single

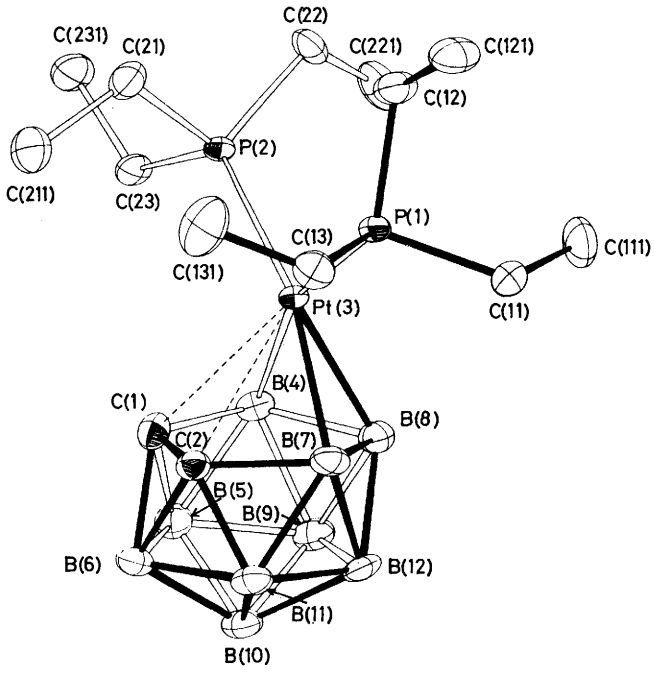

FIGURE 1 Perspective view of the molecule 3,3-$(Et_3P)_2$-3,1,2-$PtC_2B_9H_{11}$. Hydrogen atoms are omitted for clarity. Thermal ellipsoids represent 50% electron probability

molecule is given in Figure 1. Table 2 lists internuclear separations (uncorrected for libration) and Table 3 the calculated interbond angles for non-hydrogen atoms. Distance and angle data involving hydrogens are deposited as Appendices C and D respectively.

The structural analysis confirms that the platinum atom and carbaborane cage define a highly distorted icosahedral polyhedron. The main distortions may be considered as (*i*) a lateral slip of the $Pt(PEt_3)_2$ fragment across the C_2B_3 face towards the unique boron atom B(8), (*ii*) a smaller and opposite translation of the lower face, and (*iii*) a folding of the upper face with the three- and four-atom sequences B(7,8,4) and B(4)C(1,2)B(7) both tipped away from the platinum atom. The precise nature of these distortions will be discussed in more detail below.

The PtP_2 plane lies almost perpendicular to the

* For details see Notices to Authors No. 7, *J.C.S. Dalton*, 1977, Index issue.

[23] D. T. Cromer and J. T. Waber, *Acta Cryst.*, 1965, **18**, 104.
[24] D. T. Cromer and J. B. Mann, *Acta Cryst.*, 1968, **A24**, 321.
[25] R. F. Stewart, E. R. Davidson, and W. T. Simpson, *J. Chem. Phys.*, 1965, **42**, 3175.
[26] 'International Tables for *X*-Ray Crystallography,' Kynoch Press, Birmingham, 1974, vol. 4.

approximate mirror plane which passes through B(8) and the midpoint of the C(1)–C(2) bond (see Figure 2). A similar conformation has been noted for 3-Et_2NCS_2-3,1,2-$AuC_2B_9H_{11}$.[12] The internal stereochemistry of the $Pt(PEt_3)_2$ fragment closely resembles that seen in other bis(triethylphosphine)carbaplatinaborane structures.[27] Thus, one ethyl group lies effectively in the PtP_2 plane

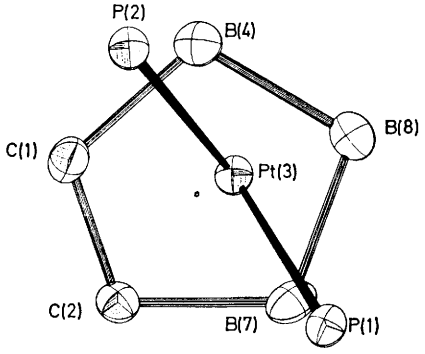

FIGURE 2 Projection of the $PtP_2C(1,2)B(7, 8, 4)$ atoms on to the plane defined by B(5, 6, 11, 12, 9), showing the slipping and orientation of the PtP_2 fragment. The centroid of the boron pentagon is represented by the small circle, and metal–cage linkages are omitted for clarity

with a torsion angle (Pt–P–C–C) close to 180° [C(12,121), C(23,231), anti-periplanar] whilst the other two are symmetrically disposed about the plane, displaying torsion angles of *ca.* 90° [C(11,111), C(22,221), (+)-clinal] and *ca.* −90° [C(13,131), C(21,211), (−)-clinal]. Thus the $Pt(PEt_3)_2$ fragment as a whole has essentially mirror symmetry and, additionally, the two PEt_3 ligands are effectively related by an in-plane rotation through the P–Pt–P angle (*ca.* 98°).

TABLE 2

Interatomic distances (Å) *

Polyhedral			
Pt(3) · · · C(1)	2.530(7)	B(8)–B(12)	1.788(12)
Pt(3) · · · C(2)	2.613(7)	B(8)–B(9)	1.786(11)
Pt(3)–B(7)	2.277(8)	B(8)–B(4)	1.803(11)
Pt(3)–B(8)	2.264(8)	B(4)–B(9)	1.812(12)
Pt(3)–B(4)	2.283(8)	B(4)–B(5)	1.804(12)
C(1)–C(2)	1.529(10)	B(5)–B(6)	1.790(12)
C(1)–B(6)	1.757(11)	B(5)–B(10)	1.801(12)
C(1)–B(5)	1.663(11)	B(5)–B(9)	1.795(12)
C(1)–B(4)	1.755(11)	B(6)–B(11)	1.764(12)
C(2)–B(6)	1.705(10)	B(6)–B(10)	1.767(12)
C(2)–B(11)	1.659(11)	B(11)–B(12)	1.791(12)
C(2)–B(7)	1.742(11)	B(11)–B(10)	1.788(11)
B(7)–B(11)	1.826(12)	B(12)–B(9)	1.751(11)
B(7)–B(12)	1.816(12)	B(12)–B(10)	1.780(12)
B(7)–B(8)	1.809(11)	B(9)–B(10)	1.769(12)
Phosphine ligands			
Pt(3)–P(1)	2.275 0(18)	Pt(3)–P(2)	2.284 3(18)
P(1)–C(11)	1.833(8)	P(2)–C(21)	1.836(8)
C(11)–C(111)	1.530(12)	C(21)–C(211)	1.530(12)
P(1)–C(12)	1.843(8)	P(2)–C(22)	1.828(8)
C(12)–C(121)	1.539(11)	C(22)–C(221)	1.516(12)
P(1)–C(13)	1.828(8)	P(2)–C(23)	1.843(7)
C(13)–C(131)	1.522(13)	C(23)–C(231)	1.531(11)

* B–H and C–H distances have been deposited.

The arrangement along each of the C–C bonds is staggered. Figure 3 views the first PCH_2CH_3 moiety down the C(111)—C(11) vector and demonstrates the ethyl-hydrogen numbering scheme used throughout.

The six P–C lengths are consistent to within *ca.* 2σ. Angles at P(2) are normal, with those involving the co-ordinate bond averaging *ca.* 12° more than the C–P–C type. At P(1) the C(12,121) ethyl group bends back to relieve contacts (g) and (h) of Table 4 and thus widens the Pt–P–C(12) angle by *ca.* 7°. Contacts (a) and (b) for the first, and (c) and (d) for the second, phosphine ligand result in relatively wide P–C(12)–C and P–C(23)–C angles, comparable with those at C(11) and C(13), but somewhat larger than those at C(21) and C(22). This latter separation of the clinal groups presumably stems from the greater ability of C(13,131) and C(11,111) to relieve interligand phosphine-phosphine contacts. Thus the C(11)–P–C(13) angle is significantly narrower than C(21)–P–C(22), with methylene-H–methylene-H contacts developing [(e) and (f) of Table 4; a consequence of the mirror symmetry of the $Pt(PEt_3)_2$ fragment is

TABLE 3

Interbond angles (°) *

Polyhedral			
C(1) · · · Pt(3) · · · C(2)	34.5(2)	C(1)–B(6)–C(2)	52.4(4)
C(2) · · · Pt(3)–B(7)	41.0(3)	C(2)–B(6)–B(11)	57.1(4)
B(7)–Pt(3)–B(8)	46.9(3)	B(11)–B(6)–B(10)	60.9(5)
B(8)–Pt(3)–B(4)	46.7(3)	B(10)–B(6)–B(5)	60.8(5)
B(4)–Pt(3) · · · C(1)	42.4(3)	B(5)–B(6)–C(1)	55.9(4)
Pt(3) · · · C(1)–C(2)	75.7(4)	C(2)–B(11)–B(7)	59.7(5)
C(2)–C(1)–B(6)	62.1(4)	B(7)–B(11)–B(12)	60.3(5)
B(6)–C(1)–B(5)	63.1(5)	B(12)–B(11)–B(10)	59.6(5)
B(5)–C(1)–B(4)	63.7(5)	B(10)–B(11)–B(6)	59.7(5)
B(4)–C(1) · · · Pt(3)	61.3(3)	B(6)–B(11)–C(2)	59.7(4)
Pt(3) · · · C(2)–C(1)	69.8(4)	B(7)–B(12)–B(8)	60.2(4)
C(1)–C(2)–B(6)	65.5(5)	B(8)–B(12)–B(9)	60.6(5)
B(6)–C(2)–B(11)	63.2(5)	B(9)–B(12)–B(10)	60.1(5)
B(11)–C(2)–B(7)	64.9(5)	B(10)–B(12)–B(11)	60.1(5)
B(7)–C(2) · · · Pt(3)	59.1(3)	B(11)–B(12)–B(7)	60.8(5)
Pt(3)–B(7)–C(2)	79.9(4)	B(8)–B(9)–B(4)	60.1(4)
C(2)–B(7)–B(11)	55.4(4)	B(4)–B(9)–B(5)	60.0(5)
B(11)–B(7)–B(12)	58.9(5)	B(5)–B(9)–B(10)	60.7(5)
B(12)–B(7)–B(8)	59.1(4)	B(10)–B(9)–B(12)	60.7(5)
B(8)–B(7)–Pt(3)	66.1(4)	B(12)–B(9)–B(8)	60.7(5)
Pt(3)–B(8)–B(7)	66.9(4)	B(4)–B(5)–C(1)	60.6(4)
B(7)–B(8)–B(12)	60.6(4)	C(1)–B(5)–B(6)	61.0(5)
B(12)–B(8)–B(9)	58.6(4)	B(6)–B(5)–B(10)	58.9(5)
B(9)–B(8)–B(4)	60.6(4)	B(10)–B(5)–B(9)	58.9(5)
B(4)–B(8)–Pt(3)	67.2(4)	B(9)–B(5)–B(4)	60.5(5)
Pt(3)–B(4)–B(8)	66.1(3)	B(6)–B(10)–B(11)	59.5(5)
B(8)–B(4)–B(9)	59.2(4)	B(11)–B(10)–B(12)	60.3(5)
B(9)–B(4)–B(5)	59.5(5)	B(12)–B(10)–B(9)	59.1(5)
B(5)–B(4)–C(1)	55.7(4)	B(9)–B(10)–B(5)	60.4(5)
C(1)–B(4)–Pt(3)	76.4(4)	B(5)–B(10)–B(6)	60.2(5)
Phosphine ligands			
	P(1)–Pt–P(2) 98.36(7)		
P(1)–Pt(3) · · · C(1)	140.34(17)	P(2)–Pt(3) · · · C(1)	100.82(17)
P(1)–Pt(3) · · · C(2)	107.61(15)	P(2)–Pt(3) · · · C(2)	126.05(15)
P(1)–Pt(3)–B(7)	89.61(20)	P(2)–Pt(3)–B(7)	166.92(22)
P(1)–Pt(3)–B(8)	114.76(20)	P(2)–Pt(3)–B(8)	135.46(21)
P(1)–Pt(3)–B(4)	161.41(20)	P(2)–Pt(3)–B(4)	98.41(20)
Pt(3)–P(1)–C(11)	110.6(3)	Pt(3)–P(2)–C(21)	115.4(3)
Pt(3)–P(1)–C(12)	122.1(3)	Pt(3)–P(2)–C(22)	116.6(2)
Pt(3)–P(1)–C(13)	112.9(3)	Pt(3)–P(2)–C(23)	113.7(2)
C(11)–P(1)–C(12)	101.4(4)	C(21)–P(2)–C(22)	105.3(4)
C(11)–P(1)–C(13)	103.5(4)	C(21)–P(2)–C(23)	101.6(3)
C(12)–P(1)–C(13)	104.4(4)	C(22)–P(2)–C(23)	102.4(3)
P(1)–C(11)–C(111)	113.1(6)	P(2)–C(21)–C(211)	111.3(6)
P(1)–C(12)–C(121)	115.0(6)	P(2)–C(22)–C(221)	112.2(6)
P(1)–C(13)–C(131)	115.2(6)	P(2)–C(23)–C(231)	116.1(5)

* Angles involving H atoms have been deposited.

[27] A. J. Welch, *J.C.S. Dalton*, (*a*) 1975, 2270; (*b*) 1977, 962.

that two pairs of methylene hydrogen atoms are mutually eclipsed].

There are four short intramolecular cage–phosphine

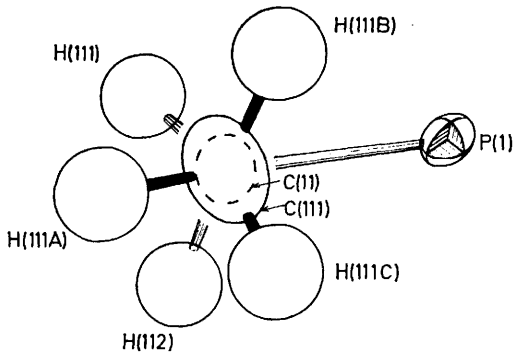

FIGURE 3 View along the C(111)–C(11) vector of the $P(1)C(11)H_2C(111)H_3$ moiety, presenting the ethyl-H numbering scheme

contacts. P(1) is locked over B(7) (see Figure 2) by (j) and (k), whilst P(2) is held above the C(1)–B(4) link by (l) and (m). Thus the PtP_2 plane is twisted by *ca.* 14° from its idealised situation perpendicular to the

TABLE 4

H · · · H Contacts [a] ⩽ 2.4 Å

Intraligand		
(a)	H(121B) · · · H(111)	2.30(19)
(b)	H(121C) · · · H(132)	2.36(19)
(c)	H(231B) · · · H(221)	2.36(18)
(d)	H(231C) · · · H(212)	2.36(18)
(e)	H(111) · · · H(132)	2.40(18)
(f)	H(112) · · · H(131)	2.37(18)
Interligand, intramolecular		
(g)	H(121) · · · H(222)	2.23(17)
(h)	H(122) · · · H(211)	2.29(18)
(i)	H(131B) · · · H(211B)	2.20(19)
(j)	H(112) · · · H(7)	2.03(18)
(k)	H(131) · · · H(7)	2.30(18)
(l)	H(231) · · · H(4)	2.36(18)
(m)	H(232) · · · H(1)	2.39(18)
Intermolecular [b]		
(n)	H(221) · · · $H(10^{I})$	2.36(18)
(o)	H(222) · · · $H(10^{I})$	2.28(18)
(p)	H(132) · · · $H(9^{II})$	2.23(18)
(q)	H(1) · · · $H(5^{III})$	2.39(18)

[a] More accurately, these distances are the separations of non-bonded centroids of electron density. True *internuclear* contacts could be up to *ca.* 0.2 Å less.[28] [b] Roman numeral superscripts define the following equivalent positions, relative to the reference molecule at *x,y,z*: I $x - \frac{1}{2}, \frac{1}{2} - y, \frac{1}{2} + z$; II $\frac{1}{2} + x, \frac{1}{2} - y, \frac{1}{2} + z$; III $-x, -y, -z$.

cage mirror plane. It is interesting to note that the rotational conformer of the moiety depicted in Figure 2 [*i.e.* P(2) above B(4), P(1) above C(2)–B(7)] would be destabilised by intramolecular contacts, by virtue of the special conformation of the $Pt(PEt_3)_2$ fragment described above.

The crystal packing is viewed along the shortest crystallographic axis in Figure 4. There are four intermolecular H · · · H contacts less than 2.4 Å (Table 4).

Definition of 'Slip' and 'Fold' Distortions.—The recent controversy surrounding the nature of distortion in these carbametallaboranes [12] prompts us to define more clearly the components of the distortion with respect to the non-bonded pentagonal girdle of the icosahedral ligand, *i.e.* atoms B(5,6,11,12,9) in Figure 1. This is essentially planar (see Table 5) and therefore serves as a reference plane for the 'slip' and 'fold' distortions. Accordingly, in Figure 5 the 'slip' distortion is defined as the distance, Δ, from the perpendicular of the reference plane to the platinum atom, this perpendicular passing through the centroid of the least-squares plane through B(5,6,11,12,9). The angles ϕ and θ define the 'fold' distortion of the bonded C_2B_3 face with respect to the perpendicular.

For $3,3\text{-}(Et_3P)_2\text{-}3,1,2\text{-}PtC_2B_9H_{11}$, Δ is calculated to be 0.42 Å, Figure 2 showing that the slip occurs in the direction of B(8), *i.e.* approximately along the effective mirror plane of the molecule. The calculated fold angles θ and ϕ are 4.7 and 4.4° respectively. Full details of the least-squares planes passing through the metal-bonded atoms and other atomic sequences are given in Table 5. In Table 6 θ, ϕ, Δ, and other selected geometrical data for a wide range of icosahedral 1,2-carbametallaboranes are summarised, together with the data for the present compound.

As we have previously noted, the slipping deformation in $(Et_3P)_2PtC_2B_9H_{11}$ is not strictly confined to movement of the metal atom, since there is a small relative slip between the upper and lower planes. With respect to the centre of the lower pentagon, the upper centroid

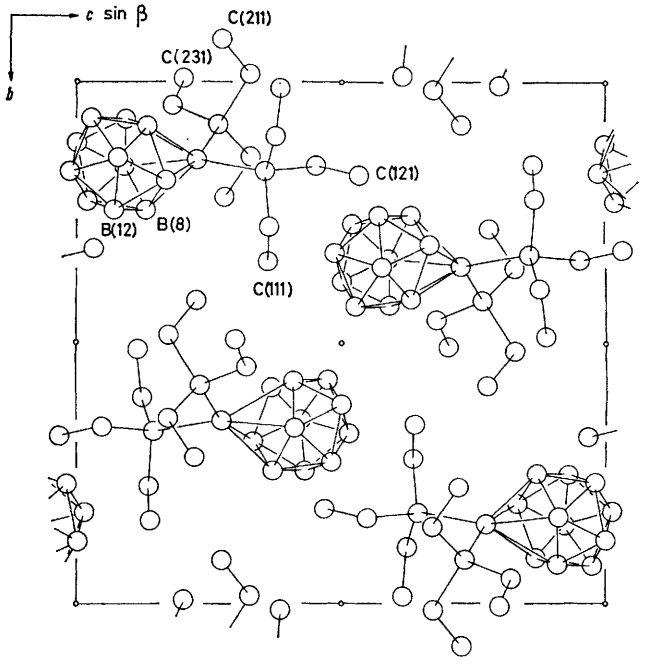

FIGURE 4 The contents of one unit cell, seen along the *a* axis, looking towards the origin. Hydrogen atoms and full cell symmetry are omitted for clarity

is displaced by *ca.* 0.10 Å [*i.e.* away from B(6)]. A re-examination of the cages listed in Table 6 reveals $B_5\text{–}C_2B_3$ interplane slips of between 0.02 and 0.10 Å.

[28] M. R. Churchill, *Inorg. Chem.*, 1973, **12**, 1213.

Δ values quoted thus fractionally overstate the movement of the metal fragment relative to the upper face.

TABLE 5

Important molecular planes *

Plane A

B(5,6,11,12,9)

$-3.916x - 2.933y + 14.656z = -0.890$

[B(5) 0.054, B(6) −0.058, B(11) 0.040, B(12) −0.006, B(9) −0.030, C(1) 1.452, C(2) 1.417, B(7) 1.584, B(8) 1.480, B(4) 1.549]

Plane B

B(4)C(1,2)B(7)

$-3.782x - 4.194y + 14.430z = 0.450$

[B(4) −0.011, C(1) 0.020, C(2) −0.020, B(7) 0.011, B(8) −0.179, Pt(3) 1.802]

Plane C

B(7,8,4)

$-4.156x - 1.781y + 14.675z = 0.838$

[C(1) −0.227, C(2) −0.282, Pt(3) 1.786]

Plane D

Pt(3)P(1,2)

$-4.386x + 14.101y + 1.339z = 1.912$

[B(7) −0.412, B(8) 1.045, B(4) 0.316]

Plane E

B(8,10,6), *i.e.* idealised cage mirror plane

$8.230x + 2.649y + 6.313z = 2.763$

Dihedral angles (°)

A–B	4.7	A–D	85.3
A–C	4.4	C–D	80.9
B–C	9.0	E–D	76.1

* Each plane is defined (in direct space) by the equation $Px + Qy + Rz = S$ Å, where x, y, and z are the atomic fractional co-ordinates. All the atoms have unit weight. Individual atomic deviations are in square brackets.

Δ is sufficiently small to classify the d^6 and d^7 ' dicarbollide ' compounds as ' unslipped '. The bonded C_2B_3 face in these complexes is nearly planar since the θ and ϕ angles are all less than 2.6°. The d^8 and d^9 ' dicarbollide ' compounds consistently have somewhat larger θ and ϕ angles {mean 6.0° except for $[Cu(B_9C_2H_{11})_2]^-$}. These compounds also show a remarkably consistent slip distortion (Δ, mean 0.5 Å).

The translational distortion in these compounds has a more important influence on the metal–boron bond lengths than does the increase in the fold angle ϕ and, as a result, M–B(8) is generally shorter than M–B(7,4) (*cf.* the unslipped molecules). In contrast, the combination of the slip distortion and the increase in θ leads to much longer metal–carbon bond lengths. The C–C bond is consistently shorter (by *ca.* 0.1 Å) in the slipped structures.

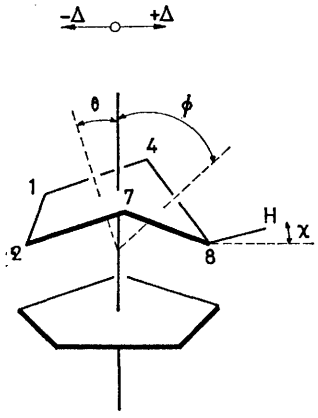

FIGURE 5 Definition of ' slip ' and ' fold ' parameters, Δ, θ, and ϕ, and the substituent elevation angle χ

The data in Table 6 clearly suggest that the electron-rich carbametallaboranes may be accurately defined as ' slipped ', in agreement with early suggestions.[10,11] The slip is also associated with a ' folding ' of the bonded pentagonal face as noted by Wallbridge and his co-workers.[12] This effect, however, is relatively minor and, indeed, is present in the unslipped structures, albeit to a lesser extent.

The elevation angles, χ, of the hydrogen substituents on the carbaborane atoms bonded to the metal in 3,3-$(Et_3P)_2$-3,1,2-$PtC_2B_9H_{11}$ are: (*i*) with respect to the BCCB plane, H(1) 31.1, H(2) 25.0, H(4) 11.0 and H(7) 19.0°; and (*ii*) with respect to the B_3 plane, H(4) 13.3, H(7) 20.0, and H(8) 18.9°, with the hydrogen atoms numbered according to the atom (B or C) to which they are bound. Since χ for a regular icosahedron is 26°, the hydrogen atoms may be generally considered to be bent back away from the metal.*

Average B–B and B–C distances in $(Et_3P)_2PtC_2B_9H_{11}$ that do not involve the upper pentagon are quite normal

TABLE 6

Geometrical data for compounds containing the 3,1,2-$MC_2B_9H_{11}$ fragment

Compound	Metal configuration	Valence electrons	θ/°	ϕ/°	Δ/Å	Bond distance/Å: |M–B(8)| − |M–B(7,4)|	Bond distance/Å: |M–B(8)| − |M–C(1,2)|	Bond distance/Å: C(1)–C(2
$[Ni(B_9C_2H_{11})_2]$ [a]	d^6	18	2.5, 2.2	0.9, 0.4	0.10, 0.09	0.03, 0.02	0.05, 0.04	1.60, 1.61
$[Re(B_9C_2H_{11})_2(CO)_3]^-$ [b]	d^6	18	1.4	−1.2	0.05	0.02	0.04	1.61
$[Ni(B_9C_2H_{11})_2]^-$ [c]	d^7	19	2.5	2.6	0.09	0.05	0.01	1.59
$[Cu(B_9C_2H_{11})_2]^-$ [d]	d^8	20	6.7, 8.4	12.0, 2.4	0.41, 0.38	0.14, −0.11	−0.36, −0.49	1.45, 1.52
$[Au(B_9C_2H_{11})_2]^-$ [e]	d^8	20	5.9	7.7	0.69	−0.06	−0.56	1.50
$[(Et_2NCS_2)Au(C_2B_9H_{11})]$ [a]	d^8	18	7.7	9.5	0.68	−0.02	−0.56	1.46
$[(Et_3P)_2Pt(C_2B_9H_{11})]$ [f]	d^8	18	4.7	4.4	0.42	−0.02	−0.31	1.53
$[Cu(B_9C_2H_{11})_2]^{2-}$ [g]	d^9	21	3.7	4.5	0.41	−0.10	−0.44	1.53

[a] Ref. 6. The cages are crystallographically independent. [b] Ref. 2. [c] Ref. 9. The molecule has precise C_{2h} symmetry. [d] Ref. 11. Each crystallographically independent molecule has imposed C_i point symmetry. [e] Ref. 12. The compound has crystallographic C_i symmetry. [f] This work. [g] Ref. 10. Precise C_i symmetry.

* Whilst internuclear distances involving H atoms located *via* *X*-ray diffraction are the subject of systematic error,[28] directional quantities (such as elevation angles) are not.

at 1.789(20) * and 1.71(5) Å respectively. B–H and C–H separations [mean 1.06(6) and 1.00(13) Å] are predictably [28] *ca.* 0.1 Å less than the accepted internuclear distance.

Molecular-orbital Analysis.—In the previous section it was established that the carbametallaborane 3,3-$(Et_3P)_2$-3,1,2-$PtC_2B_9H_{11}$ is severely distorted, and that the distortions may be separated into ' slip ' and ' fold ' components defined by the parameters Δ, θ, and ϕ. We have sought to explain the electronic origins of these distortions, using m.o. calculations based on the extended-Hückel approximation. In order to simplify the problem the initial calculations were made on the hypothetical $[(H_3P)_2PtB_{11}H_{11}]^{2-}$ ion with an idealised [*nido*-$B_{11}H_{11}]^{2-}$ icosahedral geometry. The effect of carbon substitution was then considered as a perturbation on the general bonding scheme. Also, attention will be focused initially, at least, on the more important ' slip ' distortion alone. The molecular dimensions and parameters used in the calculations are identical with those reported previously for $[(H_3P)_2PtB_{11}H_{11}]^{2-}$.[17]

The translation of the platinum atom across and parallel to the open pentagonal face of the $[B_{11}H_{11}]^{2-}$ ligand may be defined by the length Δ shown in (1).† With the bond lengths and angles chosen for the calculations, Δ values of 0.460 and 1.489 Å correspond to the metal atom lying above the B(3)–B(5) vector and above B(4) respectively [see (1)]. When $\Delta \neq 0$ the $PtB_{11}H_{11}$ moiety has a mirror plane of symmetry which can only be retained if the phosphine ligands take up perpendicular (⊥) or parallel (||) conformations with respect to this plane and are themselves related by a reflection operation, as shown in (2) and (3). In this paper the

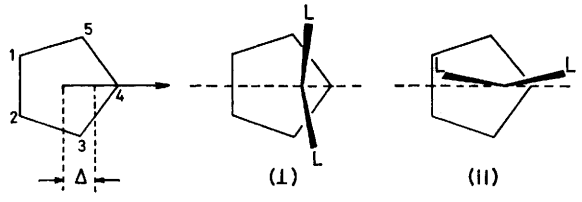

(1) (2) (3)

discussion will be limited to these symmetrical conformations.

We have previously established [17] that when $\Delta = 0.0$ these two conformations have equal energies and have suggested that the primary metal–ligand bonding effects in these complexes originate from electron donation from the ligand $6a_1$ orbital to the hybrid (*s*–*z*) lowest unoccupied molecular orbital (l.u.m.o.) of $Pt(PH_3)_2$ (4) and back donation from the $Pt(PH_3)_2$ highest occupied molecular orbital (h.o.m.o.) (5) to one component of the ligand $5e_1$ set. The metal *yz* (6) orbital enters into a four-electron destabilising interaction with the complementary (and filled) component of the $5e_1$ set.

* Estimated standard deviations of the mean from $\sigma_{mean}^2 = [\sum_{i=1}^{N}(\gamma_i - \bar{\gamma})^2]/(N-1)$, where γ_i is the *i*th and $\bar{\gamma}$ the mean of *N* similar types.

These important orbital interactions are summarised in Figure 6.

(4) (5) (6)

Before considering in detail the Walsh diagrams for the ' slip ' distortions it is instructive to qualitatively examine the variation of the $5e_1$–*xz*,*yz* overlap integrals as a function of Δ. Clearly, both the metal–ligand overlap integrals diminish as the platinum atom is moved away from the central position, but the descrease is much greater for the overlapping orbital pair (7) than (8) because the nodal planes associated with the metal and

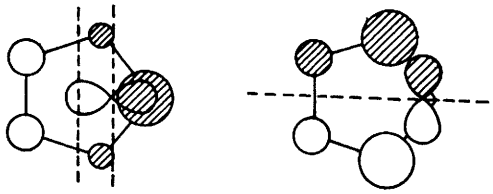

$5e_1$ (*a'*)–*xz* (7) $5e_1$ (*a''*)–*yz* (8)

ligand orbitals are no longer coincident and destructive overlap results. Indeed the overlap shown in (7) will be negligible when $\Delta = 1.5$ Å, *i.e.* metal atom above B(4).‡

For $Pt(PH_3)_2$ the orbitals having a predominance of metal *xz* and *yz* character, (5) and (6), have different overlap integrals with the ligand $5e_1$ set even when $\Delta = 0$ because of the greater directional characteristics of (5). Therefore, the translational distortion defined by Δ could serve to reinforce or diminish this difference depending on whether (5) or (6) overlaps with $5e_1(a')$ or $5e_1(a'')$. In the ⊥ conformer of $[(H_3P)_2PtB_{11}H_{11}]^{2-}$ it is the *yz* orbital which overlaps with $5e_1(a')$ (see Figure 6) and therefore the difference will be enhanced. The difference will be diminished, however, for the || conformer where it is hybrid(*xz*) which overlaps with $5e_1(a')$. The computed interfragment overlap integrals for the || and ⊥ conformers shown in Figure 7 confirm these trends and in addition suggest that the overlap between hybrid(*s*–*z*) (4) and $5e_1$ may be significant especially for large values of Δ. This overlap is precisely zero when $\Delta = 0$ for reasons for pseudo-symmetry.

Figure 8(*a*) and (*b*) indicates schematically how the changes in the $5e_1$–hybrid(*xz*),*yz* overlap integrals resulting from the ' slip ' distortion could influence the interactions between these orbitals. In order to emphasise possible trends a large value of Δ (1.5 Å) which corresponds to a negligible metal–$5e_1(a')$ overlap has

† For an undistorted icosahedral carbaborane this Δ wolud correspond precisely to that defined in Figure 5.

‡ Similar effects have been noted for CH_2 transits across a planar cyclopentadienyl ring (N. T. Anh, M. Elian, and R. Hoffmann, *J. Amer. Chem. Soc.*, 1978, **100**, 110).

been used as a limiting case. For the ⊥ conformer [Figure 8(*a*)] the important $5e_1(a'')$–hybrid (*xz*) bonding

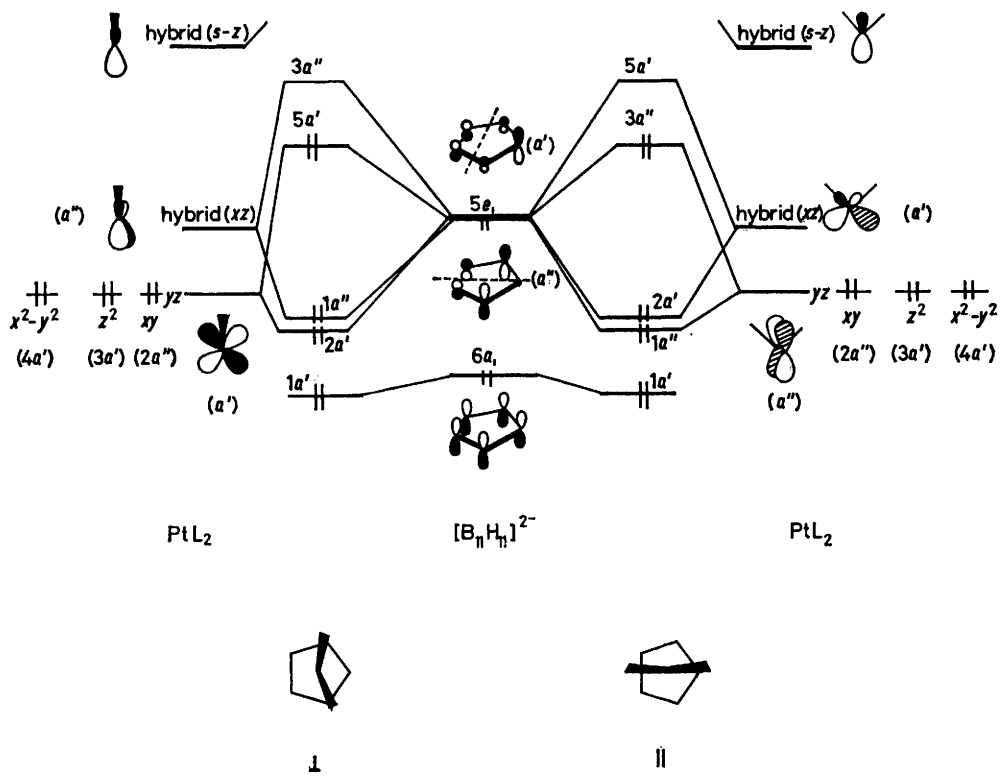

FIGURE 6 Important orbital interactions for the ⊥ and || conformations of $[(H_3P)_2PtB_{11}H_{11}]^{2-}$ when $\Delta = 0$

interaction is retained to a large extent as Δ is increased and the four-electron destabilising interaction is diminished. Indeed the latter becomes essentially non-bonding as Δ approaches 1.5 Å because of the negligible

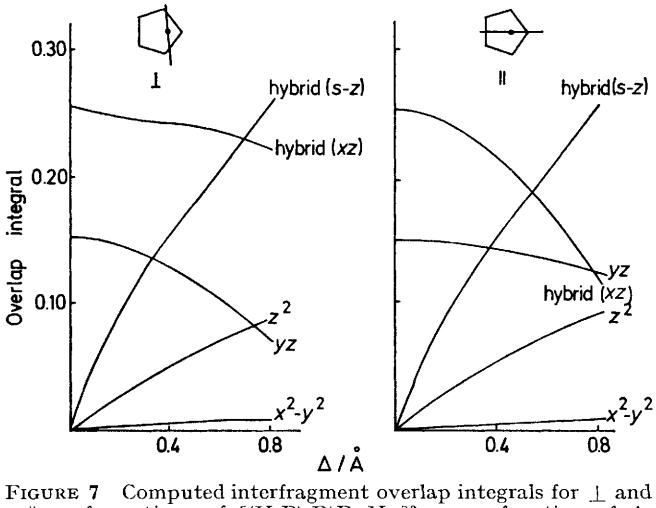

FIGURE 7 Computed interfragment overlap integrals for ⊥ and || conformations of $[(H_3P)_2PtB_{11}H_{11}]^{2-}$ as a function of Δ. The labels refer to the $Pt(PH_3)_2$ fragment m.o.s which overlap with the $5e_1$ orbitals of $[B_{11}H_{11}]^{2-}$

$5e_1(a')$–*yz* overlap. In contrast, it is the bonding $5e_1(a')$–hybrid(*xz*) interaction which is severely affected by the ' slip ' distortion in the case of the || conformer. Figure 8(*b*) suggests that as Δ approaches 1.5 Å the hybrid(*xz*)–$5e_1(a')$ pair will become essentially non-bonding. Figure 8(*a*) and (*b*) has, however, been constructed without due regard to the ' non-crossing ' rule which will lead to extensive mixing between the rising 2*a*'

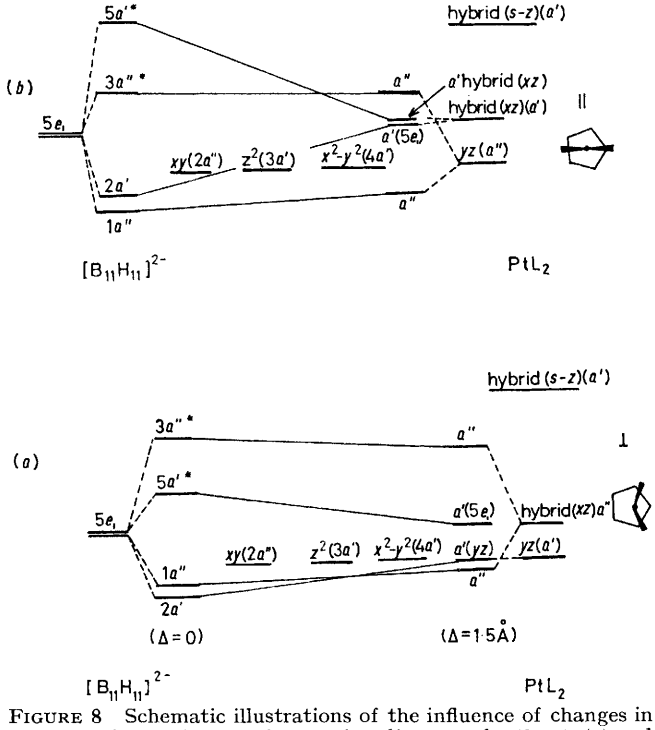

FIGURE 8 Schematic illustrations of the influence of changes in overlap integral on the interaction diagrams for the ⊥ (*a*) and || (*b*) conformations

level and the $x^2 - y^2(4a')$ and $z^2(3a')$ levels in Figure 8(*b*). When $\Delta > 0$ the z^2 orbital has a non-zero overlap with $4e_2$ and therefore significant $x^2 - y^2, z^2$ orbital mixings are also anticipated. For the $\perp$ conformer the corresponding $1a''$ [$5e_1$ + hybrid(xz)] level will not mix so extensively with the higher lying $2a''(xy)$ level because the gradient of the former is more gradual. As the distortion proceeds the interaction between $5e_1(a')$ and the higher-lying hybrid(s–z) orbital will increase reflecting the larger overlap between these orbitals (see Figure 7). The lower-lying m.o.s of a' symmetry and particularly $5a'$ will be stabilised by this interaction.

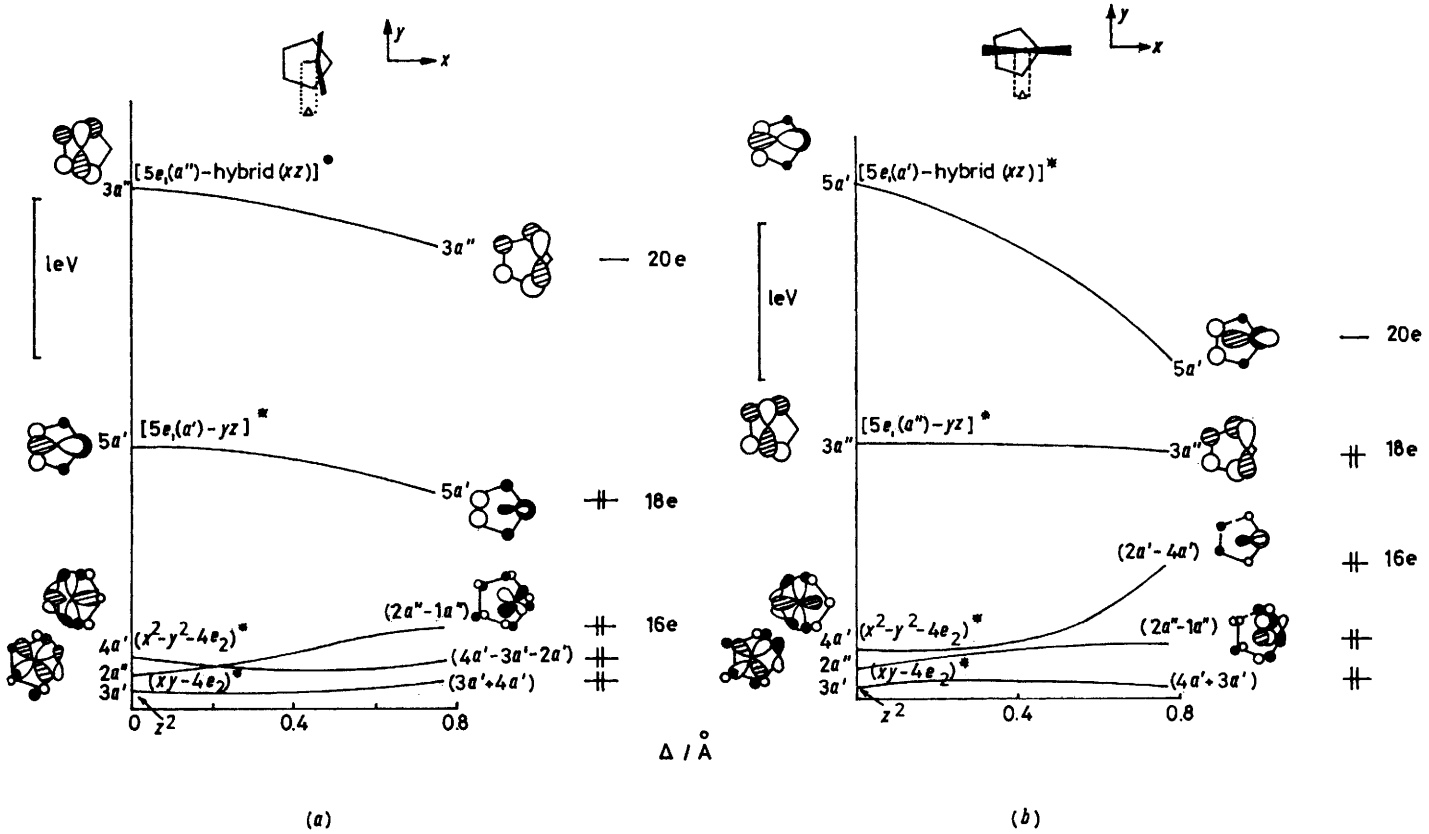

FIGURE 9 Walsh diagrams for the ' slip ' distortion in $[(H_3P)_2PtB_{11}H_{11}]^{2-}$

The Walsh diagrams derived from extended-Hückel calculations on the $\perp$ and $\parallel$ conformers shown in Figure 9 confirm the essential features of the qualitative arguments outlined above. These diagrams suggest that the propensity for the ' slip ' distortion will be dependent on the total number of valence electrons involved in metal–ligand bonding and the conformation of the ML_2 fragment. If $[B_{11}H_{11}]^{2-}$ (and isoelectronic carbaboranes) is viewed as a four-electron ligand the following generalisations arise from the Walsh diagrams. (*i*) The ' slip ' distortion is highly unfavourable for 16-electron complexes because the h.o.m.o.s, *i.e.* $(2a''$–$1a'')$ in the case of the $\perp$ conformer and $(2a'$–$4a')$ * for the $\parallel$ conformer, are destabilised by the distortion. (*ii*) For 18-electron complexes with the $\parallel$ conformation the distortion is highly unfavourable because the important hybrid(xz)–$5e_1$ bonding interaction is severely reduced. This diminishing interaction is shown as the rising $(2a'$–$4a')$ level in Figure 9(*b*). (*iii*) For 18-electron complexes with the $\perp$ conformation the potential-energy surface for the distortion is rather soft because the stabilisation of the $5a'$ level, which is a result of the smaller yz–$5e_1(a')$ overlap integral and the hybrid(s–z) interaction, is comparable to the destabilisation of the hybrid-(xz)–$5e_1(a'')$ bonding orbital $(1a'')$. In such complexes the energy minimum could be influenced by substituent effects and this aspect will be discussed in more detail below. (*iv*) The slip distortion is very favourable for 20-electron complexes with either conformation.

To date only carbametallaboranes of the type 3,3-L_2-3,1,2-$MC_2B_9H_{11}$ with 18-electron configurations have been synthesised and therefore only conclusions (*ii*) and (*iii*) above can be adequately tested. We hope the predictions inherent in (*i*) and (*iv*) will stimulate more experimental work on compounds such as $(R_3P)_2$-$RuC_2B_9H_{11}$ and $(R_3P)_2HgC_2B_9H_{11}$.

Substituent effects in 18-electron complexes. The Walsh diagram in Figure 9(*a*) for the $\perp$ conformer of $[(H_3P)_2PtB_{11}H_{11}]^{2-}$ suggests that the energetics of the ' slip ' distortion are finely balanced because of the opposing gradients of the $5a'$ and $(2a''$–$1a'')$ levels,

* The orbital mixings between $2a''$ and $1a''$, $2a'$ and $4a'$, *etc.* resulting from ' avoided crossings ' are denoted by $(2a''$–$1a'')$, $(2a'$–$4a')$, *etc.* in Figure 9(*a*) and (*b*).

and therefore if the relative gradients of these levels could be changed the distortion could be encouraged. The $5a'$ level in Figure 9(*a*) is the antibonding component of the $5e_1$–yz interaction when $\Delta = 0$, but as the metal atom is displaced from the central position the $5e_1$–yz overlap decreases and the m.o. becomes more localised on the ligand. In addition the orbital is stabilised by an interaction with hybrid(s–z). The increase in electron density on the ligand is not uniformly distributed amongst all the boron atoms in the open pentagonal face and the calculated orbital populations illustrated in (9) and (10) indicate a build-up of electron density on boron atoms 1 and 2, *i.e.* those atoms which are farthest from the metal atom. Similar effects have been noted for the rising ($2a''$–$1a''$) level in Figure 9(*a*).

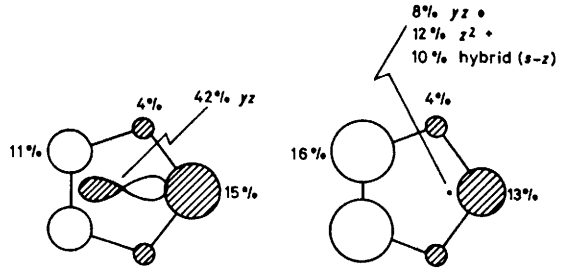

$\Delta = 0$ (9) $\Delta = 0.8$ Å (10)

This redistribution of electron density is reflected in the total charge distribution (expressed in electrons) in the $[(H_3P)_2PtB_{11}H_{11}]^{2-}$ ion as estimated from a Mulliken population analysis and given in (11) and (12)

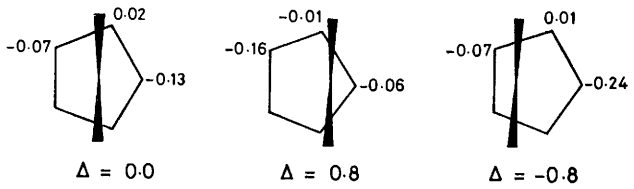

$\Delta = 0.0$ (11) $\Delta = 0.8$ (12) $\Delta = -0.8$ (13)

below. Molecular-orbital calculations for the alternative ' slip ' distortion which leads to negative values of Δ have also been completed and indicate a similar trend, *i.e.* a build up of negative charge at the boron atom farthest from the metal [see (13) for example]. First-order perturbation-theory arguments [29] suggest that electronegative substituents (or heteroatoms) at those positions where there is a build up of negative charge will encourage the ' slip ' distortion. This leads to the prediction that complexes based on the carbaborane ligands 1,2-$C_2B_9H_{11}$ and $[1\text{-}CB_{10}H_{11}]^-$ should have ' slipped ' structures and furthermore the direction of ' slip ' will be opposite, *i.e.* $+\Delta$ for the former and $-\Delta$ for the latter.

It has been noted above that the ' slip ' distortion is less favourable for the $\parallel$ conformer of $[(H_3P)_2PtB_{11}H_{11}]^{2-}$ and therefore substituent effects will be less important for such complexes. The influence of substituents on the direction of the ' slip ' distortion may be predicted

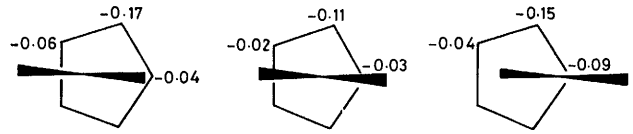

$\Delta = -0.8$ (14) $\Delta = -0.0$ (15) $\Delta = 0.8$ (16)

on the basis of the calculated atomic charges for $\Delta = -0.8$, 0.0, and 0.8 Å shown above. Clearly the introduction of two electronegative heteroatoms in non-adjacent positions in the open pentagonal face of the $[B_{11}H_{11}]^{2-}$ ligand could encourage a small negative ' slip ' distortion.

The first-order perturbation-theory arguments outlined above neglect changes in the $[B_{11}H_{11}]^{2-}$ ligand wavefunctions which will also be associated with the introduction of heteroatom substituents. In particular, they neglect changes in metal–ligand overlap integrals resulting from the redistribution of electron density in the ligand h.o.m.o.s. The metal–ligand overlap populations calculated for the $\perp$ conformer (Table 7) of

TABLE 7

Calculated overlap populations of the $\perp$ conformer of $[(H_3P)_2PtB_{11}H_{11}]^{2-}$ as a function of Δ for the ligand $5e_1$ orbitals

	Δ/Å		
Overlapping orbitals	0.0	0.4	0.8
hybrid (xz)–$5e_1(a'')$	0.41	0.39	0.34
hybrid (s–z)–$5e_1(a')$	0.00	0.06	0.17
yz–$5e_1(a')$	−0.04	−0.03	−0.01
$x^2 - y^2$–$5e_1(a')$	0.00	−0.002	−0.002
z^2–$5e_1(a')$	0.00	−0.003	−0.001
xy–$5e_1(a'')$	0.00	0.002	0.004

$[(H_3P)_2PtB_{11}H_{11}]^{2-}$ confirm that the ' slip ' distortion is dominated by the interactions of the ligand $5e_1$ orbitals with the metal hybrid(xz) and hybrid(s–z) orbitals, *i.e.* the h.o.m.o. and l.u.m.o. of the $Pt(PH_3)_2$ fragment. Therefore the changes introduced into the $[B_{11}H_{11}]^{2-}$ ($5e_1$) wavefunctions by the carbon substituents can to a good approximation be followed by considering the frontier-orbital interactions between the h.o.m.o.s and l.u.m.o.s of the carbaborane and metal-containing fragments.

Figure 10 represents schematically the effect of carbon substitution on the energies and compositions of the $5e_1$ levels of $[B_{11}H_{11}]^{2-}$. Substitution of the carbon atoms removes the degeneracy of the $5e_1$ levels and the relative orders of the resulting a' and a'' levels may be readily calculated from first-order perturbation theory.[17] The polarisation effects resulting from substitution may be estimated from second-order perturbation theory. The representations in the Figures are derived from extended-Hückel calculations on these carbaboranes based on an idealised icosahedral geometry.[17] The frontier orbitals of the $Pt(PH_3)_2$ fragment are shown on

[29] E. Heilbronner and H. Bock, ' Das H.M.O.-Modell und Seine Anwendung,' Verlag Chemie, Weinheim, 1968.

the right-hand side of the Figure. The conformations of the $Pt(PH_3)_2$ complexes derived from the ligands in Figure 10 are decided primarily by the metal–ligand h.o.m.o.–l.u.m.o. interactions which are maximised when the nodal planes of the interacting pair of m.o.s are in coincidence, *i.e.* when the ML_2 fragment lies perpendicular to the mirror plane of symmetry in the case of (1) and (3) and parallel to the plane in (2).

For the parent $[B_{11}H_{11}]^{2-}$ ligand the metal h.o.m.o.–ligand l.u.m.o. overlap is largest when the metal atom lies above the centre of the pentagonal face. This is not the case for the less symmetrical carbaborane ligands and the first-order perturbation-theory arguments. Therefore, both the electronegativity and overlap effects encourage the ' slip ' distortions in complexes based on $1,2\text{-}C_2B_9H_{11}$ and $[CB_{10}H_{11}]^-$.

For the alternative isomer of $C_2B_9H_{11}$ [(2) in Figure 10] a negative ' slip ' distortion is indicated by the localisation of the l.u.m.o. at the 1,2 positions, but the magnitude of the distortion is limited by the loss of coincidence of the metal and ligand nodal planes as the distortion proceeds. This conclusion is also in accord with that derived from the perturbation-theory arguments given above.

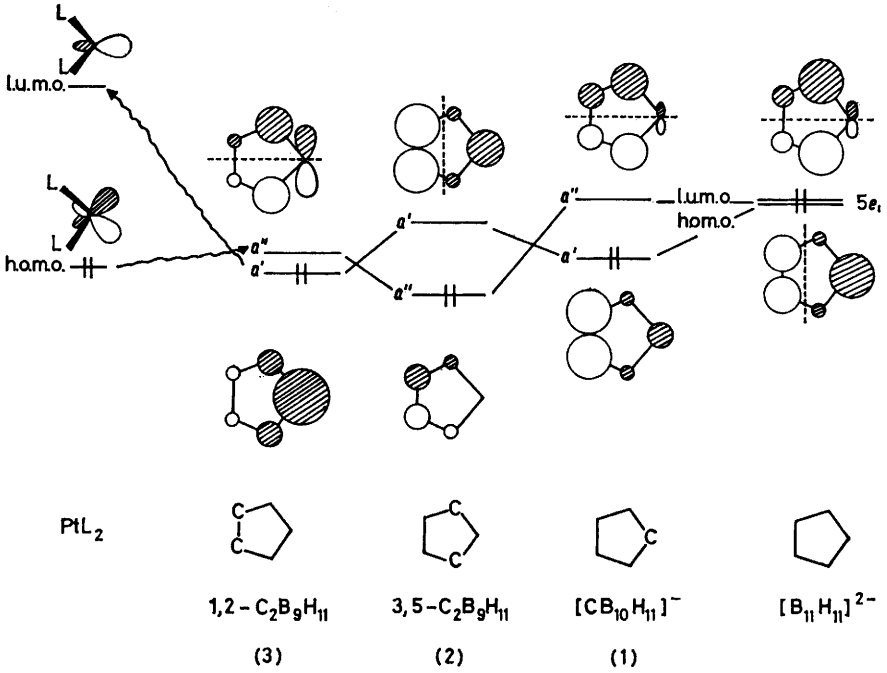

FIGURE 10 Schematic representation of the effect of carbon substitution on the h.o.m.o. and l.u.m.o. of $[B_{11}H_{11}]^{2-}$ and their interactions with hybrid(xz) and hybrid(s–z) of $Pt(PH_3)_2$

because carbon substitution has the effect of localising the ligand frontier orbitals on to the boron atoms of the open pentagonal face. These localisation effects are represented schematically in Figure 10. The metal–ligand h.o.m.o.–l.u.m.o. interactions are increased by a negative ' slip ' for the $[CB_{10}H_{11}]^-$ complex because of the pronounced localisation at the 1,2 positions. For $C_2B_9H_{11}$ (3) the increased localisation at the 4 position in the h.o.m.o. and the 3,5 positions in the l.u.m.o. encourage a positive 'slip'. The following $Pt(PH_3)_2$–$C_2B_9H_{11}$ interfragment overlap integrals underline the importance of the hybrid(s–z)–$5e_1(a')$ interaction and the fact that the maximum hybrid(xz)–$5e_1(a'')$ overlap is no longer achieved when $\Delta = 0$:

	Δ/Å		
Overlap integrals	0.0	0.4	0.8
S [hybrid (xz)–$5e_1(a'')$]	0.186	0.199	0.196
S [hybrid (s–z)–$5e_1(a')$]	0.251	0.359	0.422
S [yz–$5e_1(a'')$]	0.120	0.088	0.037

These conclusions are in complete agreement with those derived above on the basis of the Walsh diagrams

The results of the m.o. calculations on $(H_3P)_2Pt\text{-}C_nB_{11-n}H_{11}$ compounds may be summarised as follows:

Ligand	Predicted conformation	Slip distortion
(1) $[CB_{10}H_{11}]^-$	⊥	large $-\Delta$
(2) $C_2B_9H_{11}$	∥	small $-\Delta$
(3) $C_2B_9H_{11}$	⊥	large $+\Delta$

X-Ray crystallographic studies on $1\text{-}Me_3N\text{-}2,2\text{-}(Bu^tNC)_2\text{-}2,1\text{-}PdCB_{10}H_{10}$ (A), $1,1\text{-}(PhMe_2P)_2\text{-}2,4\text{-}Me_2\text{-}1,2,4\text{-}PtC_2B_9H_9$ (B), and $3,3\text{-}(Et_3P)_2\text{-}3,1,2\text{-}PtC_2B_9H_{11}$ (C) (present work) are in complete accord with these conclusions. The relevant distortion parameters (Table 8) confirm that the direction of ' slip ' in (A) and (C) is opposite and that Δ is much larger for these compounds than for (B). The dihedral angles in Table 8 indicate that the non-planarity of the ligand face arises in each case from a movement of the carbon atoms away from the metal atom and towards the non-bonded pentagonal girdle of atoms. The localisation effects indicated in Figure 10 can be held responsible for these distortions, because the larger atomic coefficients at the boron atoms lead to

larger metal–boron overlap populations. Therefore the ' slip ' and ' fold ' distortions observed in these complexes can be simply understood in terms of the theoretical model which has been developed above.

A remaining point which needs to be clarified concerns the observation that although the 18-electron compound 3,3-$(Et_3P)_2$-3,1,2-$PtC_2B_9H_{11}$ has a large ' slip ' distortion, the related 18-electron $[3,3,3\text{-}(OC)_3\text{-}3,1,2\text{-}ReC_2B_9H_{11}]^-$ shows only a small value of Δ of *ca.* 0.05 Å. The reason for this difference has been sought in the different orbital compositions and populations of the $Re(CO)_3$ and $Pt(PH_3)_2$ fragments. Detailed derivations of the m.o.s of a $M(CO)_3$ fragment having C_{3v} symmetry have been given elsewhere. Such a fragment has three essentially non-bonding m.o.s $a_1(z^2)$ and $1e(x^2 - y^2,xy)$, and three higher-lying frontier orbitals $a_1(s\text{–}z)$ and $2e(xz,yz)$.[30-33] It is the last orbitals [illustrated in (17) and (18) below] which determine the stereochemistries of $M(CO)_3$ complexes.

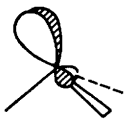

2e(a'') (17)

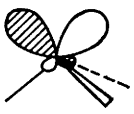

2e(a') (18)

For a d^8 metal ion, as in $[Re(CO)_3]^-$ or $Os(CO)_3$, the $M(CO)_3$ frontier orbitals have electron populations $(2e)^2$-$[a_1(s\text{–}z)]^0$. The $2e$ molecular orbitals are ideally suited to enter into a pair of two-electron stabilising bonding interactions with the $5e_1$ ligand set of $[B_{11}H_{11}]^{2-}$, or the related orbitals of the carbaborane ligands shown in Figure 10. For $[B_{11}H_{11}]^{2-}$ these bonding interactions will clearly be maximised when $\Delta = 0.0$ Å, and are little altered by the substitution effects noted previously. Clearly this situation is quite different to that discussed above for the $Pt(PH_3)_2$ fragment where the metal yz orbital enters into a four-electron destabilising interaction with one component of the ligand $5e_1$ set.

A comparison of the bond lengths in the ' slipped ' and ' unslipped ' complexes suggests that a shortening of the C–C bond length by *ca.* 0.1 Å accompanies the slip distortion (see Table 6). The Mulliken overlap populations calculated for 3,3,3-$(OC)_3$-3,1,2-$OsC_2B_9H_{11}$ and 3,3-$(H_3P)_2$-3,1,2-$PtC_2B_9H_{11}$ have reproduced this trend [see (19) and (20)]. The larger C–C overlap population can be attributed primarily to the higher electron population of the $5e_1(a')$ level in the platinum complex. This orbital is noded between the B–C bonds and therefore this analysis suggests that the shortening of the C–C bond should be accompanied by a lengthening of the B–C bond. These effects have indeed been noted by other workers and most recently by Wallbridge and his co-workers.[12]

TABLE 8

Summary of distortion parameters Δ, ϕ, and θ

Compound	Ligand [a] type	Δ/Å	ϕ/°	θ/°	Bond length/Å M–4	M–3,5 [b]	M–1,2 [b]	Conformation
(A)	(1)	−0.32	12	4	*2.600(6)*	2.250(7)	2.241(8)	⊥
(B)	(2)	−0.13	−11	−5	2.270(9)	*2.447(8)*	2.258(9)	∥
(C)	(3)	0.42	4	5	2.264(8)	2.280(8)	*2.572(7)*	⊥

[a] See Figure 10 for definition. [b] Mean values. The values in italics refer to metal–carbon bonds, the remainder to metal–boron.

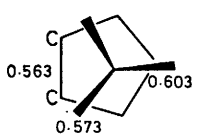

$(OC)_3OsC_2B_9H_{11}$

(19)

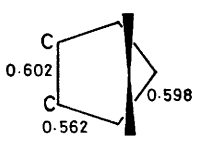

$(H_3P)_2PtC_2B_9H_{11}$

Δ = 0·4

(20)

We have also recently completed m.o. calculations on the ' sandwich ' complexes $[M(B_9C_2H_{11})_2]^{n-}$ and these results will be discussed in a subsequent publication.

We thank the S.R.C. for the award of a research studentship to (M. I. F.), Dr. J. L. Spencer for crystals of the title compound, and Professor M. G. H. Wallbridge for some of his unpublished crystallographic data and for many useful discussions.

[7/1551 *Received*, 31*st August*, 1977]

[30] M. Elian and R. Hoffmann, *Inorg. Chem.*, 1975, **14**, 1058.
[31] M. Elian, M. M. L. Chen, D. M. P. Mingos, and R. Hoffmann, *Inorg. Chem.*, 1976, **15**, 1148.
[32] J. K. Burdett, *J.C.S. Faraday II*, 1974, 1599.
[33] T. A. Albright, P. Hofmann, and R. Hoffmann, *J. Amer. Chem. Soc.*, 1977, **99**, 7546.